

Understanding the effect of doping on the charging performance of the Li-O₂ battery: the role of hole polarons and lithium vacancies

Henry A. Cortes,[†] Jhon F. Zapata,^{‡,¶} María A. Barral,^{‡,¶} and Verónica L.

Vildosola^{*,‡,¶}

[†]*Departamento de Química Inorgánica, Analítica y Química Física/INQUIMAE, Facultad de Ciencias Exactas y Naturales, Universidad de Buenos Aires, Ciudad Universitaria, Pab. II, Buenos Aires C1428EHA, Argentina*

[‡]*Departamento de Física de la Materia Condensada, Gerencia de Investigación y Aplicaciones, Comisión Nacional de Energía Atómica, Av. General Paz 1499, (1650) San Martín, Pcia. de Buenos Aires, Argentina*

[¶]*Instituto de Nanociencia y Nanotecnología, Comisión Nacional de Energía Atómica and Consejo Nacional de Investigaciones Científicas y Técnicas*

E-mail: vildosol@tandar.cnea.gov.ar

Abstract

In this work, we perform DFT calculations using the hybrid functional HSE to properly describe the insulating nature of lithium peroxide and study its more energetically favourable surfaces [0001], [1 $\bar{1}$ 00] and [11 $\bar{2}$ 0]. We then analyse how the insulating character and the correct description of the hole polarons at the Li₂O₂ surfaces affect the electrochemical steps of Li₂O₂ decomposition in the charging process of the Li-O₂ battery. We then study the effect of doping and propose possible scenarios in which

the ions as Na^+ or K^+ dissolved in the electrolyte can dope and promote Li vacancies generation in the Li_2O_2 that, in turn, reduce the energy barrier of the limiting steps of the Li_2O_2 decomposition. The origin of this reduction are the lattice distortions associated with doping that weaken the surface binding.

Introduction

The Li- O_2 battery (LOB) is a promising energy storage system due to its exceptionally high theoretical energy density ($\sim 3500 \text{ Whkg}^{-1}$).^{1,2} However, the LOBs technology is still facing important challenges and limitations that have to be sorted out. Among them, there are the high charging potential that leads to low discharge/charge cycle efficiency, the reduced capacity at high discharge rates and the poor cathode and electrolyte stability.^{2,3}

The main discharge product of the LOB is Li_2O_2 whose insulating character deeply affects various aspect of the battery.^{2,4,5} The dominant reversible reaction that takes place at the cathode of a non-aqueous Li- O_2 cell is



During the discharge of the battery, the oxygen from the air is reduced at the cathode and combines with a Li ion to form solid Li_2O_2 . During the recharge, the reverse decomposition of Li_2O_2 occurs. The overpotential needed to recharge the battery determines its efficiency and depends on several factors that can have different origin. The source of the energy barriers originates in the intrinsic reversible reaction but also is affected by the morphology of the discharge product^{2,6} or the presence of side-reaction secondary phases.^{5,7}

A profound knowledge of the electronic and transport properties of Li_2O_2 both in bulk and at the surface is crucial to understand the reversible reaction of Eq. 1 and to propose new routes to circumvent the above mentioned difficulties.

The charge transport through the bulk of Li_2O_2 has been studied extensively by ex-

periments and theoretical calculations.⁸⁻¹³ Particularly, Gerbig *et al.* observed the Li_2O_2 insulating nature by impedance spectroscopy and DC conductivity measurements, showing that ionic lithium defects are the majority carriers while electronic conductivity is two order of magnitude smaller and of hole type. These results were confirmed later by Dunst *et al.* by means of nuclear magnetic resonance spectroscopy.⁹ Independently, Ceder and coworkers showed, using Density Functional Theory (DFT) calculations with the Heyd-Scuseria-Ernzerhof (HSE) screened hybrid functional, that holes can be self-trapped at the peroxide sites (O_2^{-2}) forming small hole polarons (O_2^{-1}). Furthermore, they noted that the nonpolaronic structure, which present metallic states, has significantly higher energy than the polaronic one.¹¹ Afterwards, Radin and Siegel, employing the same hybrid functional, concluded that the dominant charge carriers in bulk Li_2O_2 are the lithium vacancies (V_{Li}) and hole polarons, and that the inclusion of exact exchange at some extent is essential for achieving their correct description.¹³

Li_2O_2 surfaces have also been object of study as possible conduction paths during the operation of the cell. Previous theoretical reports have shown that the more energetically favourable surface of Li_2O_2 under ambient conditions is metallic.¹⁴ These results were based on DFT calculations using functionals in the General Gradient Approximation (GGA). A metallic behaviour of the Li_2O_2 surface would have deep consequences in the performance of the LOB since it could mitigate the electrical passivation of the cathode. Furthermore, the important role played by the Li_2O_2 surfaces in the oxygen evolution reaction (OER) occuring during the recharge of the battery has also motivated experimental and theoretical research.¹⁵⁻¹⁹ Resorting to DFT calculations in the GGA approximation, Mo *et al.* studied the energetics and the OER for different surface orientations.¹⁶ Afterwards, Hummelshøj *et al.* investigated the electrochemical mechanism of growth and dissolution over the $[1\bar{1}00]$ Li_2O_2 facet, the more stable one using the revised PBE functional (RPBE), analysing possible origins of the overpotential. Based on these RPBE calculations where the intermediate lithium vacancies in the OER reaction give rise to surface metallic states, they conclude that

the electron transport through the Li_2O_2 may not be a problem at the high potentials.¹⁷

In view of the well known self-interaction error of the GGA functional, the result of the surface metallicity was revisited²⁰ using the HSE correction and even the scGW method.²⁰ Interestingly, the metallic behaviour that was also obtained for these corrected functionals, arises as an artifact due to a finite size effect of a small 1x1 unit cell that does not allow for surface reconstruction. In fact, calculations done later for larger supercells and proper functionals confirm that all the Li_2O_2 surfaces are insulating and that the only charge carrier conduction path available is the diffusion of defects²¹ or through tunnelling in the case of thin films.²² Considering the very high computational cost of HSE, specially for simulating large supercells, the DFT+U technique²³ was also used as an alternative to correct the underestimation of the electronic correlation characteristic of local or semilocal functionals as GGA.¹²

After this winding road towards understanding the formation and decomposition of Li_2O_2 in the LOB, there is still some confusion in the literature regarding these fundamental issues that hinders future efforts to make progress in this promising technology and a clarification is urging.

With respect to the high charging overpotential, several strategies were proposed. Recently, Byon and coworkers showed that the nanostructuring of one-dimensional and amorphous Li_2O_2 can get an improve of the round-trip efficiency of the LOB of $\sim 80\%$. DFT calculations reveal that the structural distortions of the amorphous structure lead to a weaker binding of LiO_2 , a key intermediate in the reaction, yielding smaller overpotentials in the delithiation process.²⁴

On the other hand, the Li_2O_2 doping has been reported as another potential strategy to improve the efficiency of the LOB.²⁵⁻³⁰ However, the mechanisms of how the incorporation of heteroatoms in the Li_2O_2 can affect performance of the battery is still unclear. Experimentally, barium (Ba) was one of the heteroatoms considered, achieving a significant reduction in the charging overpotential. The authors ascribed this effect to an improvement in the

charge transport as a consequence of Ba incorporation in Li_2O_2 .²⁸ Afterward, Chen and coworkers showed that a LOB with Na-doped Li_2O_2 as a discharge product also presents a lower charge overpotential as compared to the undoped system, since the Na^+ as the dopant induces lithium vacancies, which according their DFT calculations, lead to conducting states in Li_2O_2 .²⁹ Nevertheless, in view of the above mentioned problems of self-interaction errors, this theoretical interpretation needs to be revised.

Quite recently, Chen and coworkers synthesized K-doped Li_2O_2 , detecting an increment of O_2^- sites and Li vacancies. Compared to the pristine Li_2O_2 , the as-prepared defective Li_2O_2 was also shown to give rise to lower overpotentials during the OER. Additionally, they showed that there is a strong correlation between the OER kinetics and the O_2^- density in the discharge products and that those O_2^- sites highly contribute to the decrease of charge overpotential.³⁰

The available reported values of the calculated overpotentials present considerable dispersion and they sometimes match with the ones experimentally observed and sometimes not. As said before, the absolute value of this quantity depends on many factors. Some of them have to do with variables that not always are considered in the theoretical calculations such as the characteristic of the electrolyte, the presence of complex extended defects, the presence of undesired secondary products or particular of the experimental setup. Other factors of technical origin are directly related to the particular model considered to describe the discharge product. For instance, the theoretical overpotential value strongly depends on the exchange and correlation functional, on the supercell size, on the calculation of the oxygen molecule chemical potential and the criteria to correct the well known overbinding error of GGA functionals. Despite this, if all these technicalities are properly taken into account, we believe that DFT can still provide deep understanding of the underlying mechanism of the Li_2O_2 formation and decomposition in the LOB and it is a powerful tool to propose new routes to face the limitations of this promising technology.

In this work, we provide an insightful description of the electronic and structural prop-

erties of the more energetically favourable Li_2O_2 surfaces obtained with the HSE functional, modeling the supercell that allow for the polaron formation not only for in non-stoichiometric surfaces but also during all the electrochemical steps involved in the recharge of the battery. We study the effect of the insulating nature of the surface in the lithium peroxide decomposition and how doping can induce lower energy barriers to decrease the charging overpotential.

Computational methods

First-principle calculations are performed with the generalized gradient corrected approximation (GGA) by Perdew, Burke and Ernzerhof (PBE), as well as the hybrid functional by Heyd, Scuseria and Ernzerhof (HSE06), as implemented in the Vienna ab initio simulation package. A mixing coefficient $\alpha=0.48$ is used for the HSE hybrid calculation, in order to reproduce the bandgap obtained with more accurate techniques as G_0W_0 and self-consistent GW.¹³ DFT+U corrections within the VASP code have also been considered and analysed.

The Kohn–Sham equations are solved employing the projected augmented wave (PAW) method. The Li (2s) and O (2s, 2p) valence electrons are treated with a plane wave cutoff of 400 eV. The k-point meshes with the Monkhorst–Pack scheme for the $[0001]$, $[1\bar{1}00]$ and $[1\bar{2}00]$ surface supercells are $3\times 6\times 1$, $2\times 6\times 1$ and $4\times 3\times 1$, respectively.

The ionic relaxations of the internal positions of the slabs are performed for fixed lattice constants¹ until residual forces are below 0.02 eV/Å, with a total energy precision of 10^{-6} eV.

The surfaces are simulated using a slab geometry of Li_2O_2 separated by a vacuum layer of 10 Å in the $[0001]$, $[1\bar{1}00]$, and $[11\bar{2}0]$ directions. In some cases, it is necessary to duplicate the cell in one direction of the surface plane and remove selected lithium or oxygen atoms in order to attain different surface stoichiometries such as the oxygen rich (O-rich) and stoichiometric one (ST). The lithium rich stoichiometry is not considered in the present work because it is

¹The lattice parameters are obtained from a full cell relaxation using GGA with a cutoff of 600 eV, getting $a=3.16$ Å and $c=7.69$ Å in good agreement with previous calculations and experimental results.^{14,31}

more energetically unstable.²¹

The surface energy, for T=300 K and P =1 atm, can be calculated as:

$$\gamma(T, P) = \frac{1}{2A} [G^{slab}(T, P, N_{Li}, N_O) - \frac{1}{2} N_{Li} g_{Li_2O_2}^{bulk}(T, P) + (N_{Li} - N_O) \mu_O(T, P)], \quad (2)$$

where G^{slab} is the free energy of the surface supercell, A is the area of the exposed surface, N_{Li} and N_O are the numbers of Li and O atoms present in the slab, $g_{Li_2O_2}^{bulk}(T, P)$ is the free energy per formula unit of bulk Li_2O_2 and $\mu_O(T, P)$ are the chemical potentials of O in bulk Li_2O_2 . We neglect vibrational contributions to the free energy of the condensed phases and approximate the free energies G^{slab} and $g_{Li_2O_2}^{bulk}(T, P)$ with the DFT ground-state total energies E^{slab} and $E_{Li_2O_2}$, respectively. The chemical potential of oxygen is set by assuming equilibrium with O_2 gas at ambient conditions. To correct the well known oxygen overbinding error, the same approach as in Ref. 13 was employed, obtaining a correction of 740 meV and 630 meV using GGA and HSE($\alpha=0.48$), respectively.

We calculate the free energy of each electrochemical intermediate step during the recharge process of the battery, following the approach as outline in Ref. 17. It is assumed that the couple ($Li^+ + e^-$) is in equilibrium with bulk metallic Li; that the O_2 molecule in solution is in equilibrium with both, O_2 in the gas phase and O_2 adsorbed at the surface; that during the desorption of Li^+ ion at the cathode there is a coordinated $Li^+ + e^-$ charge transfer and that the interactions of the surface species with the electrolyte can be ignored. Furthermore, we consider that the Li_2O_2 dissolution occurs mainly on the Li_2O_2 surface rather than near the cathode.

The free energy change between reaction steps is given by:

$$\Delta G_n = [E_n - E_{n-1} + \Delta N_{Li}(\mu_{Li} - eU) + \Delta N_{O_2} \mu_{O_2}], \quad (3)$$

where n represents an intermediate reaction step, E_n is the total energy of the configuration at the step n , ΔN_{Li} and ΔN_{O_2} are the number of Li and O_2 atoms that are removed from

the surface in the step n respect to the step $(n - 1)$, and eU is electron energy under the applied charging potential U .

Results and discussion

Surface energy and electronic structure

First, we calculate the surface energy and the electronic structure of the $[0001]$, $[1\bar{1}00]$ and $[11\bar{2}0]$ facets with different stoichiometries, which were previously reported as the most stable ones.^{14,18,21} Figure 1 shows the crystal structure of the studied surfaces for the stoichiometric and oxygen rich situations (ST and O-rich) obtained with HSE. The formation of polarons occurs for the non-stoichiometric cases within HSE. Precisely, the lacking charge at the oxygen rich surfaces takes the form of hole polarons at certain dimers, that are sketched as purple bonded O_2 in Figure 1.

It can be observed that all the O-rich orientations calculated using HSE exhibit hole polarons at their surface layers. The non-compensated charge due to the missing Li atoms gets self-trapped at the surface O_2 dimers. On the other hand, the ST ones do not show this effect.

Table 1 presents the calculated surface energies corresponding to the cases shown in Figure 1, obtained for $T=300$ K and $P=1$ atm, using both GGA and HSE. The γ energies are in good agreement with previous reports.^{14,21}

Table 1: Surface energies γ of Li_2O_2 at 300 K and 1 atm, the * denoted the lowest surface energy within each method.

Orientation	Termination	γ^{GGA}	γ^{HSE}
		[meV/Å ²]	[meV/Å ²]
[0001]	O-rich-1	17.0*	50.8
	ST-4	47.8	44.2
[1 $\bar{1}$ 00]	O-rich-2	31.5	43.7
	ST-3	33.5	37.5*
[11 $\bar{2}$ 0]	O-rich-1	40.4	49.4
	O-rich-2	34.3	50.4

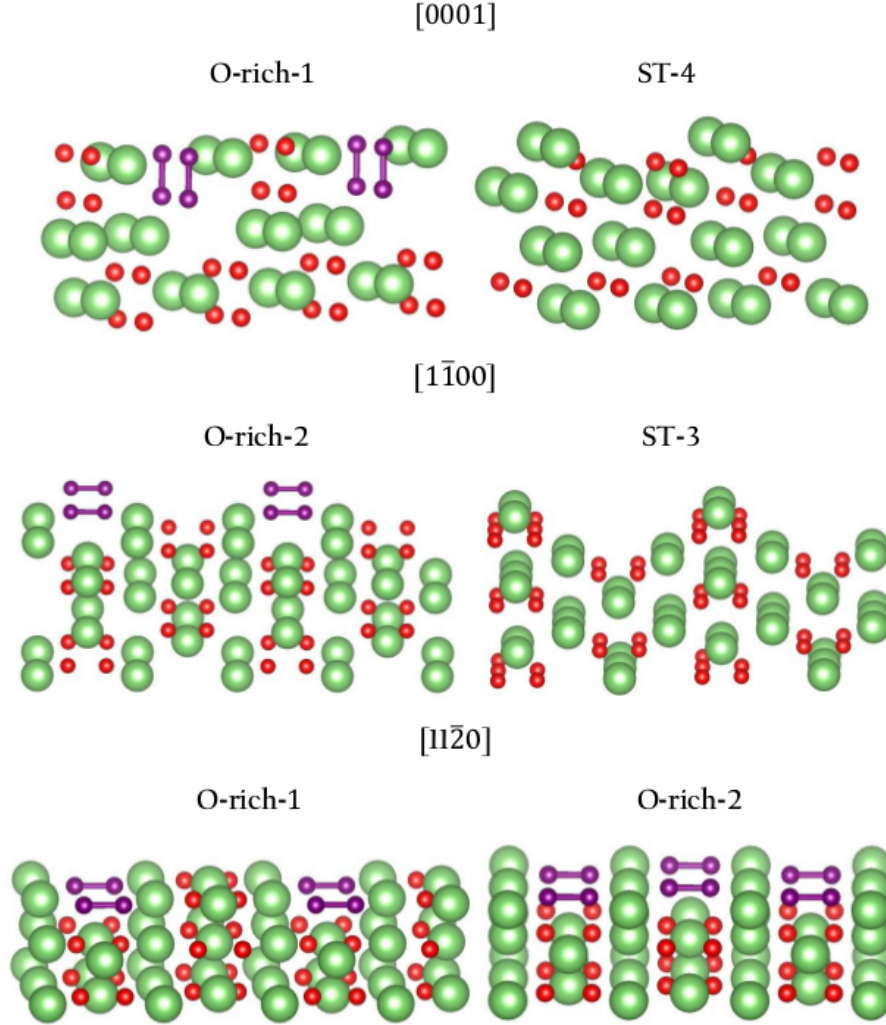


Figure 1: Crystal structure of Li_2O_2 surfaces with their corresponding termination calculated with HSE. Red and green spheres represent O and Li atoms, respectively, and the dimer sketched with a purple bond represents a hole polaron localized at the O_2 site.

From Table 1, it can be seen how GGA and HSE provide a qualitatively different thermodynamic description of the trend in the stability of the surfaces. Within GGA the most stable orientation is the $[0001]$ O-rich-1 while within HSE it is the $[1\bar{1}00]$ ST-3 one. The discrepancy between GGA and HSE arises from the fact that GGA is not able to correctly describe the localization of the non-compensated charge (the hole polarons) due to the intrinsic self-interaction error. The functional HSE partially corrects this error by adding a fraction of exact exchange and it is able to achieve the formation of hole polarons. These polarons have an elastic cost which rises the surface energy γ , therefore, it is expected that

the O-rich facets have higher γ than the ST ones within HSE.

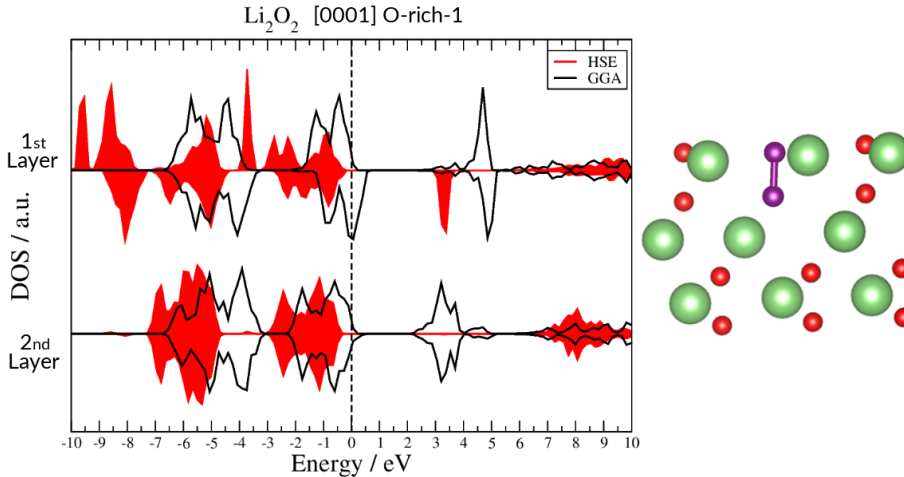


Figure 2: (Left) DOS calculated using GGA (black line) and HSE (solid red) projected to the whole 1st and 2nd layers of the surface [0001] O-rich-1, top and bottom panels, respectively. (Right) Crystal structure of the corresponding surface calculated within HSE.

Figure 2 shows the DOS calculated using GGA (black line) and HSE (solid red line) projected on the atoms of the 1st and 2nd layers of the [0001] O-rich-1 surface, top and bottom panels, respectively. As can be observed in the figure, according to GGA, this O-rich surface turns out to be metallic and with spin polarized oxygen p -states in the 1st layer. The same happens for the rest of the O-rich facets studied. This is a consequence of the tendency of the GGA functional to spuriously delocalize the charge, being in this case holes, since the number of O atoms is greater than the number of Li ones. On the other hand, the 2nd layer remains insulating with a band-gap similar to the obtained for the bulk.^{11,20,27} Conversely, the same surface calculated within HSE turns out to be insulating. In this case the holes get localized in the form of polarons, which structurally is evidenced by the reduction of bond-length in one of the surface dimer from $d_{o-o} = 1.47 \text{ \AA}$ that is the bond-length for O_2^{-2} to $d_{o-o} = 1.31 \text{ \AA}$ for O_2^- . The corresponding projected DOS shows that the polaron states lie in the band-gap of the 1st layer (solid red in Figure 2).

The polaron formation at the O-rich surface emerges as a consequence of a surface reconstruction, which in Ref. 14 was blocked by using a 1x1 supercell. Breaking the symmetry

using a 2x1 unit cell, the reconstruction is now possible and the polaron is stabilized being $30.3 \text{ meV}/\text{\AA}^2$ more stable than the delocalized configuration. The same effect occurs for Li_2O_2 bulk, where the extra charge also prefers to be localized at the oxygen dimers.^{11,13,27}

On the other hand, Figure 3 presents the DOS calculated within GGA (black line) and HSE (solid red) for the whole 1st and 2nd layers of the $[1\bar{1}00]$ ST-3 surface, the one with the lowest γ using HSE. Unlike the O-rich surfaces, in the ST ones there are not extra charge that can be self-trapped to produce polarons. In this case, it can be observed an insulating behavior with both methods (GGA and HSE), and the same happens to all stoichiometric situations.

Non of the studied surfaces are metallic within HSE. These results confirm the strong insulating character of Li_2O_2 , that is one of the main drawbacks of the LOB.

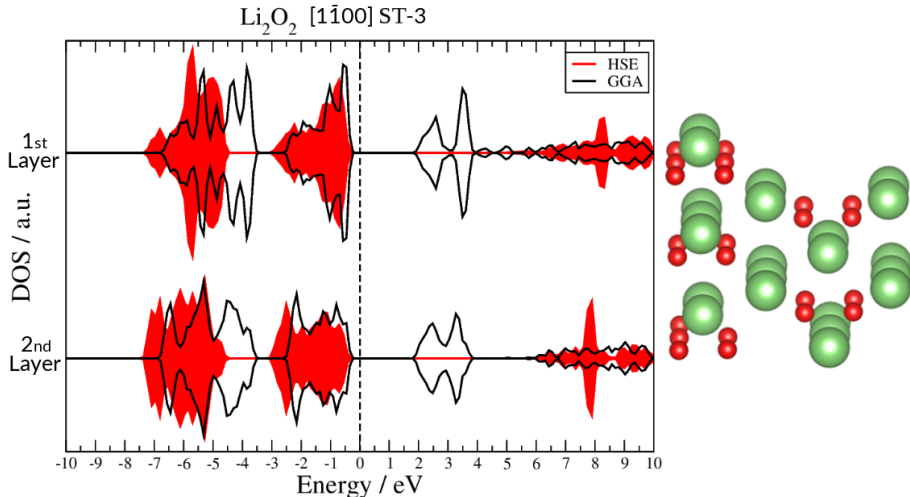


Figure 3: (Left) DOS calculated with GGA (black line) and HSE (solid red) of the whole 1st and 2nd layers of the surface $[1\bar{1}00]$ ST-3. (Right) Crystal structure of the corresponding surface calculated with HSE.

DFT+U corrections applied to Li_2O_2

The DFT+U technique has been also used to study Li_2O_2 as a less computationally demanding method to correct the well known problems of the GGA functionals.

Previously, it has been reported that DFT+U calculations as implemented in the GPAW

code,³² are able to describe the stabilization of hole polarons in Li_2O_2 for physically relevant values of the Hubbard U parameter.^{12,33} However, as mentioned later in Ref. 34, care should be taken when applying DFT+ U techniques to extended orbitals as the p states. For instance, in the VASP code, the implemented DFT+ U formalism is sensitive to the PAW augmentation radius that it might be smaller than the spatial extension of the orbital that one intends to correct. On the other hand, the GPAW implementation of the DFT+ U reduces the effect of the augmentation radius dependence by normalizing the integral of the projected atomic orbitals within the augmentation sphere, scaling the corresponding overlaps accordingly.

In this work, we aim to assess the effect of the DFT+ U correction as implemented in the widely used VASP code when applied to extended p -states as the ones present in Li_2O_2 .²³ For this, we vary the U parameter between 0 and 16 eV in order to observe the effect of the Hubbard correction on the crystalline and electronic structure for Li_2O_2 bulk and its more stable surfaces.

Since the final conclusion of this assessment is that applying the U correction to the extended p -states of lithium peroxide gives rise to unrealistic situations, we present the whole analysis in the Supplementary Information (SI) material and summarise here the main findings.

From the bulk calculation, it is observed that the DFT+ U correction is not able to reproduce the band-gap value of other more precise calculation techniques such as HSE or scGW. Furthermore, it is shown that a minimum value of $U = 8$ eV is necessary to stabilize the hole polarons and avoid spurious metallic solutions. In turn, these unphysical large values of U affect dramatically the formation energy and migrations barriers of the intrinsic defects, which could lead to wrong interpretations of the charge transport in the Li_2O_2 . Regarding the calculations of the Li_2O_2 surface energies, the thermodynamic description obtained with DFT+ U is different from that obtained with both GGA and HSE. This difference could be ascribed to the artificial reconstructions induced by the high U required to stabilize the polaron.

From a technical point of view, our calculations indicate that the DFT+U correction as implemented in the VASP code, is not appropriate for correcting GGA deficiencies in Li_2O_2 . From now on, we continue presenting the results obtained with HSE in comparison with GGA.

Li_2O_2 decomposition during the charging process

Now we discuss the reaction energy profile of the OER for the surface with the lowest γ according to HSE, the $[1\bar{1}00]$ ST-3. The reaction free energy was calculated using Eq. 3. Figure 4 shows the results obtained for a potential $U=0\text{V}$, using the GGA (black line) and HSE (red line) functionals. First of all, at $U=0\text{V}$, as expected, the whole reaction is endothermic. In both methods, the initial step in the reaction path is the formation of a lithium vacancy (V_{Li}). Within GGA the extra charge left behind by V_{Li} is wide spread along the surface, the surface turns metallic in this step. See the corresponding DOS in Figure S5 in the SI file. On the contrary, a hole gets trapped at a surface O_2 dimer within HSE, forming a polaron. This step has a higher energy barrier within HSE than within GGA, since the former functional leads to an extra elastic cost. The polarons are again schematized as purple bonded O_2 dimers in the insets of Figure 4. The second step is the formation of a second V_{Li} that gives rise to another polaron within HSE whereas within GGA more metallic states are generated (see Figure S5 in the in SI file). In general, the second V_{Li} has a lower formation energy than the first one because the surface structure was already distorted by the first vacancy; the system is less bound. The subsequent two reaction steps are the liberation of two LiO_2 . It is important to remark that these steps present a higher energy barrier for the functional GGA. The reason for this is that the energy cost is comparatively larger within GGA due to the overbinding energy of the delocalized charge. On the other hand, within HSE the system gets rid of the elastic cost of one polaron in each of the last two steps so that the final reaction free energy turns out to be smaller than within GGA.

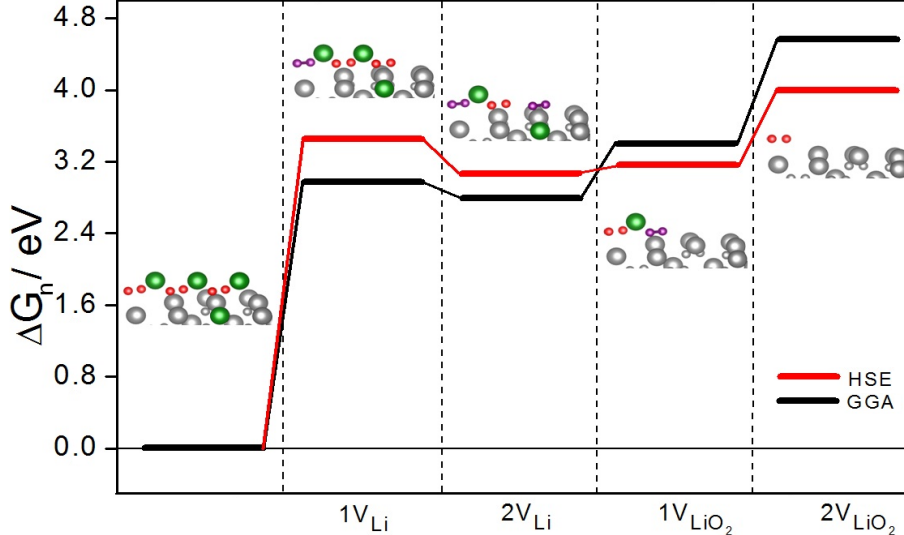


Figure 4: Reaction free energy diagram during OER calculated with GGA (black line) and HSE (red line), at $U= 0V$. Lithium in dark gray (bulk) and light green (to be removed); oxygen dimer in bulk (dark gray), to be removed (light red) and the O_2^- (light purple).

In particular, the last step is the limiting one and will determine the value of the overpotential. In the present work, we do not aim to obtain an absolute value of the overpotential because we are not considering other complex details such as the role of the solvent, the Li and O_2 diffusion and charge transport through the Li_2O_2 , among others. The main message of this section is that some care should be taken when describing the recharge process within GGA because the energy cost of the limiting step is overestimated.

Effect of doping in the Li_2O_2 decomposition

In the previous section we have clarified the electronic structure and the energetics of the Li_2O_2 surface and its mechanism for the delithiation in the recharge process of the LOB. We used a proper functional for the exchange and correlation potential as HSE that corrects the self-interaction error introduced by the standard GGA. In the present section, we proceed to study the effect of Na doping in the OER. As mentioned in the Introduction, Chen and coworkers showed a decrease in the charging overpotential when Na^+ ions were dissolved in the electrolyte, doping the formed Li_2O_2 in the LOB.²⁹ The explanation of this desired effect

was ascribed to the generation of more lithium vacancies in the presence of Na^+ that supposedly gives rise to metallic states as described by their DFT calculations. These calculations were performed using HSE with $\alpha=0.207$ for which the obtained insulating band gap of ~ 4 eV is still lower than the one calculated with $\alpha=0.48$ and the more accurate formalism GW (~ 6 eV), indicating that the theoretical metallic states obtained in the presence of lithium vacancies with $\alpha=0.207$ are an artifact because the self-interaction correction is not completely accomplished.

In this work, we study the effect of Na^+ doping in the electronic structure and the OER of the more stable Li_2O_2 surface using HSE with $\alpha=0.48$. The experiment performed by Chen and coworkers shows that the increased amount of Na^+ doping produces higher oxidation states of oxygen indicating a transition tendency from O_2^{-2} to O_2^- associated to the presence of more lithium vacancies in the Li_2O_2 deposit.

That the Na^+ doping promotes the generation of lithium vacancies can be first checked by comparing the V_{Li} formation energy obtained with and without Na^+ for the $[1\bar{1}00]$ ST-3 surface. We explore different Li^+ substitutional sites for Na doping (see Figure S6 and Table S2 in the SI material). For the more energetically stable Na-doping site, we calculate the lithium vacancy energy formation for different remaining Li^+ sites (see Figure S7 and Table S3 in the SI file). In line with the experimental observation, the formation energy in the presence of Na^+ for the more favorable vacancy site is 150 meV smaller than for the pristine surface (see Table S3 in the SI file).

There is another scenario in which dissolved Na^+ can promoted lithium vacancies. If an electrolyte with high donor number is used in the experiment, as was the case of Ref. 29, the solution mechanism of Li_2O_2 formation in the LOB is more likely.³⁵

Considering the solution mechanism, two LiO_2 dissolved in the electrolyte disproportionate to form Li_2O_2 releasing one O_2 molecule. As mentioned before, the doping with K^+ has also been probed to promote the tendency to O_2^- and the generation of lithium vacancies.³⁰

In general, when a cation X is dissolved in the electrolyte, the following disproportionation

is expected $\text{XO}_2 + \text{LiO}_2 \rightarrow \text{LiXO}_2 + \text{O}_2$.

We first calculate the energetics of the disproportionation when X is equal to Li, Na and K for comparison. The corresponding disproportionation energy reads:

$$E_{dis} = (E_{LiXO_2} + E_{O_2}) - (E_{LiO_2} + E_{XO_2}) \quad (4)$$

In Figure 5, we show the three cases studied and their calculated $E_{dis}(\text{X})$. We obtain $E_{dis}(\text{Li}) < E_{dis}(\text{Na}) < E_{dis}(\text{K})$. So that we conclude that the disproportionation of LiO_2 with NaO_2 and KO_2 are less energetically favorable than with LiO_2 . In this scenario, the eventual non-disproportionated NaO_2 and KO_2 might get trapped in the Li_2O_2 deposits where Na^+ or K^+ occupy a Li^+ crystal site next to an associated O_2^- . This frustrated disproportionation of NaO_2 or KO_2 concomitantly generates a V_{Li} nearby.

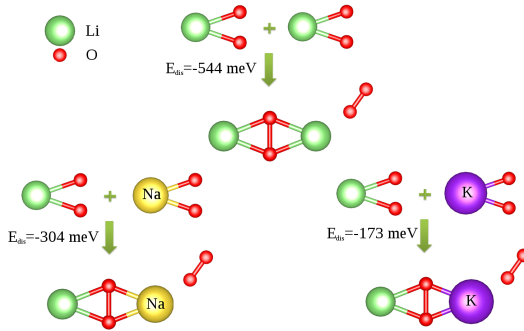


Figure 5: Schema and disproportionation energies E_{dis} of LiO_2 with LiO_2 , NaO_2 and KO_2 .

Considering as a fact that Na^+ or K^+ doping promotes V_{Li} generation, we next focus on the Na^+ case to study the OER for the Na-doped $[1\bar{1}00]$ ST-3 surface in the presence of one V_{Li} as initial state. In this Section, we will only show the results obtained with HSE $\alpha=0.48$. The initial state of the simulated OER process for the Na-doped surface is depicted in the inset a) of Figure 6. It can be observed that there are a Na surface ion (in yellow), a hole polaron at the surface dimer O_2 (in purple) and the initial lithium vacancy is indicated with a cross. As mentioned before, we remark that both the Na substitutional site and the initial lithium vacancy are the ones that resulted more energetically stable.

Figure 6 shows the calculated reaction free energy of the OER process at $U=0$ V for the

Na-doped Li_2O_2 surface (blue line) in comparison with the corresponding for the pristine Li_2O_2 (red line). We can see that the energy cost of taking out the Li in the first step is considerable smaller in the Na-doped surface. The reason for this is that the doped case presents an initial level of distortion that makes this surface less bound. Similar arguments are valid for the following steps of the OER process. The main results of this study is that the more limiting step of the OER, that is, the last LiO_2 removal, presents a sensible reduction (266 meV for the simulated supercell) for the doped case as compared to the pristine surface. It is important to remark that the reduction of the energy barriers is not a consequence of the emerging metallic states as it has been claimed in the literature. We confirm that the poor electronic conductivity of lithium peroxide even at its surfaces is one of the main limitations for the operation of the LOBs. The effect of Na-doping induces structural distortions by promoting lithium vacancies and will also improve the electronic conductivity mediated by polarons as suggested in Refs. 36,37 for amorphous Li_2O_2 , both effects turning beneficial for the Li_2O_2 decomposition during the recharge process.

Interestingly, similar conclusions pointing to the decrease in the overpotential as a consequence of a decrease in the binding energy of the intermediate LiO_2 have been reported for one-dimensional nanostructured amorphous Li_2O_2 .²⁴

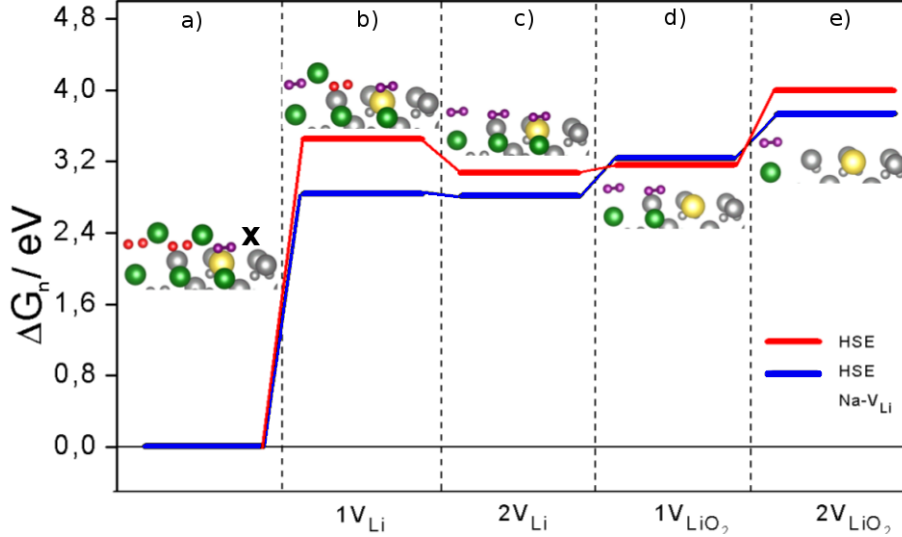


Figure 6: Reaction free energy diagram during OER calculated with HSE for Li_2O_2 (red line) and $\text{Li}_2\text{O}_2\text{-Na}$ doped (blue line), at $U=0\text{V}$. Lithium in dark gray (bulk) and light green (to be removed); oxygen in dark gray (bulk), light red (to be removed), light purple (O_2^-) and light yellow Na.

In this line, our results suggest that K-doping will be even more effective in reducing the overpotential since more lithium vacancies and more structural distortions are expected for this heavier heteroatom.

It is worth mentioning that when these calculations of the OER are performed with GGA, we also obtain an improvement of the OER barrier (731 meV for the simulated supercell) for the Na-doped surface as compared to the pristine one. However, this energy gain is strongly overestimated as a consequence of the GGA overbinding of the pristine Li_2O_2 surface.

Conclusions

In this work, we have studied the electronic structure of different Li_2O_2 surfaces using the hybrid functional HSE that is capable of adequately describing the electronic structure and modeling the localization of hole polarons. The insulating nature of the all studied surfaces has been confirmed. In the non-stoichiometric terminations with low-coordinated surface oxygen atoms, we have also confirmed a similar charge self-trapping behaviour as found in Li_2O_2 bulk. Then, we have examined the Li_2O_2 decomposition that occurs during the

recharge process using HSE to take into account the presence of the surface polarons in the electrochemical intermediate steps. These results have been compared with the ones obtained using the GGA functional, which tend to delocalize the excess of charge carriers. We have shown that the free energy variation of the limiting step is overestimated within GGA when there are spurious metallic states instead of hole polarons.

Finally, we have investigated the Na-doping effect on the lithium vacancy generation and on the Li_2O_2 surface decomposition. On the one hand, it is found that Na dopant reduces the lithium vacancy formation energy compared to the value for pristine surface, promoting the vacancy generation in agreement with experimental results. On the other hand, we have presented a plausible scenario to enhance lithium vacancies when the formation of the lithium peroxide occurs via a solution mechanism and Na^+ or K^+ ions are dissolved in the electrolyte. Based on the analysis of the energetics for different superoxide disproportionations, we have proposed that NaO_2 formed in the electrolyte can get trapped on the discharge product, concomitantly with the formation of a lithium vacancy. We have also predicted that K-doping should be even more efficient in reducing the overpotential than Na-doping.

At last, the Na-doped Li_2O_2 decomposition has been studied. The removal of the second LiO_2 intermediate is found to be the limiting step during charge, in both Na-doped and pristine Li_2O_2 surfaces. We have found that Na-doping decreases the energy barrier of the limiting step, contributing to a reduction of the charging overpotential, in line with the experimental results. Our calculations indicate that the origin of this decrease are the lattice distortions associated with doping that weaken the LiO_2 binding, and not the emergence of surface metallic states as previously reported.

Acknowledgement

The authors received financial support from PICTs 2015-0869, PICT-2016-0867 and 2019-02128 of ANPCyT, Argentina.

Supporting Information Available

In the Supplementary information file we include:

- Detailed results of the DFT+U calculations performed with the VASP code.
- DOS plot of each electrochemical step of the Li_2O_2 decomposition reaction calculated with GGA and HSE ($\alpha=0.48$).
- The crystal structure of with the different sites evaluated for the dopants and lithium vacancies and their corresponding energy of formation.

References

- (1) Imanishi, N.; Luntz, A. C.; Bruce, P. *The Lithium Air Battery: Fundamentals*; Springer, 2014.
- (2) Aurbach, D.; McCloskey, B. D.; Nazar, L. F.; Bruce, P. G. Advances in understanding mechanisms underpinning lithium–air batteries. *Nat. Energy* **2016**, *1*, 1–11.
- (3) Luntz, A. C.; McCloskey, B. D. Nonaqueous Li-Air Batteries: A Status Report. *Chem. Rev.* **2014**, *114*, 11721–11750.
- (4) Viswanathan, V.; Thygesen, K. S.; Hummelshøj, J. S.; Nørskov, J. K.; Girishkumar, G.; McCloskey, B. D.; Luntz, A. C. Electrical conductivity in Li_2O_2 and its role in determining capacity limitations in non-aqueous Li- O_2 batteries. *J. Chem. Phys.* **2011**, *135*, 214704.
- (5) McCloskey, B. D.; Burke, C. M.; Nichols, J. E.; Renfrew, S. E. Mechanistic insights for the development of Li- O_2 battery materials: addressing Li_2O_2 conductivity limitations and electrolyte and cathode instabilities. *Chem. Commun.* **2015**, *51*, 12701–12715.

- (6) Adams, B. D.; Radtke, C.; Black, R.; Trudeau, M. L.; Zaghbi, K.; Nazar, L. F. Current density dependence of peroxide formation in the Li-O₂ battery and its effect on charge. *Energy Environ. Sci.* **2013**, *6*, 1772–1778.
- (7) Horwitz, G.; Calvo, E. J.; Leo, L. P. M. D.; de la Llave, E. Electrochemical stability of glyme-based electrolytes for Li-O₂ batteries studied by infrared spectroscopy. *Phys. Chem. Chem. Phys.* **2020**, *22*, 16615–16623.
- (8) Gerbig, O.; Merkle, R.; Maier, J. Electron and Ion Transport in Li₂O₂. *Adv. Mater.* **2013**, *25*, 3129–3133.
- (9) Dunst, A.; Epp, V.; Hanzu, I.; Freunberger, S. A.; Wilkening, M. Short-range Li diffusion vs. long-range ionic conduction in nanocrystalline lithium peroxide Li₂O₂-the discharge product in lithium-air batteries. *Energy Environ. Sci.* **2014**, *7*, 2739–2752.
- (10) Wang, J.; Zhang, Y.; Guo, L.; Wang, E.; Peng, Z. Identifying Reactive Sites and Transport Limitations of Oxygen Reactions in Aprotic Lithium-O₂ Batteries at the Stage of Sudden Death. *Angew. Chem. Int. Ed.* **2016**, *55*, 5201–5205.
- (11) Ong, S. P.; Mo, Y.; Ceder, G. Low hole polaron migration barrier in lithium peroxide. *Phys. Rev. B* **2012**, *85*, 081105.
- (12) Garcia-Lastra, J. M.; Myrdal, J. S. G.; Christensen, R.; Thygesen, K. S.; Vegge, T. DFT+U Study of Polaronic Conduction in Li₂O₂ and Li₂CO₃: Implications for Li-Air Batteries. *J. Phys. Chem. C* **2013**, *117*, 5568–5577.
- (13) Radin, M. D.; Siegel, D. J. Charge transport in lithium peroxide: relevance for rechargeable metal-air batteries. *Energy Environ. Sci.* **2013**, *6*, 2370–2379.
- (14) Radin, M. D.; Rodriguez, J. F.; Tian, F.; Siegel, D. J. Lithium Peroxide Surfaces Are Metallic, While Lithium Oxide Surfaces Are Not. *J. Am. Chem. Soc.* **2012**, *134*, 1093–1103.

- (15) Seriani, N. Ab initio thermodynamics of lithium oxides: from bulk phases to nanoparticles. *Nanotechnology* **2009**, *20*, 445703.
- (16) Mo, Y.; Ong, S. P.; Ceder, G. First-principles study of the oxygen evolution reaction of lithium peroxide in the lithium-air battery. *Phys. Rev. B* **2011**, *84*, 205446.
- (17) Hummelshøj, J. S.; Blomqvist, J.; Datta, S.; Vegge, T.; Rossmeisl, J.; Thygesen, K. S.; Luntz, A. C.; Jacobsen, K. W.; Nørskov, J. K. Communications: Elementary oxygen electrode reactions in the aprotic Li-air battery. *J. Chem. Phys.* **2010**, *132*, 071101.
- (18) Hummelshøj, J. S.; Luntz, A. C.; Nørskov, J. K. Theoretical evidence for low kinetic overpotentials in Li-O₂ electrochemistry. *J. Chem. Phys.* **2013**, *138*, 034703.
- (19) Lee, B.; Seo, D.-H.; Lim, H.-D.; Park, I.; Park, K.-Y.; Kim, J.; Kang, K. First-Principles Study of the Reaction Mechanism in Sodium–Oxygen Batteries. *Chem. Mater.* **2013**, *26*, 1048–1055.
- (20) Radin, M. D.; Tian, F.; Siegel, D. J. Electronic structure of Li₂O₂ {0001} surfaces. *J. Mater. Sci.* **2012**, *47*, 7564–7570.
- (21) Radin, M. D. *First-Principles and Continuum Modeling of Charge Transport in Li-O₂ Batteries*; University of Michigan: Ann Arbor, MI, 2014.
- (22) Luntz, A. C.; Viswanathan, V.; Voss, J.; Varley, J. B.; Nørskov, J. K.; Scheffler, R.; Speidel, A. Tunneling and Polaron Charge Transport through Li₂O₂ in Li–O₂ Batteries. *J. Phys. Chem. Lett.* **2013**, *4*, 3494–3499.
- (23) Dudarev, S. L.; Botton, G. A.; Savrasov, S. Y.; Humphreys, C. J.; Sutton, A. P. Electron-energy-loss spectra and the structural stability of nickel oxide: An LSDA+U study. *Phys. Rev. B* **1998**, *57*, 1505–1509.
- (24) Dutta, A.; Wong, R. A.; Park, W.; Yamanaka, K.; Ohta, T.; Jung, Y.; Byon, H. R.

- Nanostructuring one-dimensional and amorphous lithium peroxide for high round-trip efficiency in lithium-oxygen batteries. *Nat. Commun* **2018**, *9*, 680.
- (25) Radin, M. D.; Monroe, C. W.; Siegel, D. J. How Dopants Can Enhance Charge Transport in Li_2O_2 . *Chem. Mater.* **2015**, *27*, 839–847.
- (26) Matsuda, S.; Kubo, Y.; Uosaki, K.; Hashimoto, K.; Nakanishi, S. Improved Energy Capacity of Aprotic Li-O₂ Batteries by Forming Cl-Incorporated Li_2O_2 as the Discharge Product. *J. Phys. Chem. C* **2016**, *120*, 13360–13365.
- (27) Cortes, H. A.; Vildosola, V. L.; Barral, M. A.; Corti, H. R. Effect of halogen dopants on the properties of Li_2O_2 : is chloride special? *Phys. Chem. Chem. Phys.* **2018**, *20*, 16924–16931.
- (28) Matsuda, S.; Uosaki, K.; Nakanishi, S. Improved charging performance of Li-O₂ batteries by forming Ba-Incorporated Li_2O_2 as the Discharge Product. *J. Power Sources* **2017**, *353*, 138–143.
- (29) Lyu, Z.; Wang, T.; Guo, R.; Zhou, Y.; Chen, J.; Wang, X.; Lin, M.; Tian, X.; Lai, M.; Peng, L.; Wang, L.; Peng, Z.; Chen, W. Promoting defective- Li_2O_2 formation Na doping for Li-O₂ batteries with low charge overpotentials. *J. Mater. Chem. A* **2019**, *7*, 10389–10396.
- (30) Dai, W.; Cui, X.; Chi, X.; Zhou, Y.; Yang, J.; Lian, X.; Zhang, Q.; Dong, W.; Chen, W. Potassium Doping Facilitated Formation of Tunable Superoxides in Li_2O_2 for Improved Electrochemical Kinetics. *ACS Appl. Mater. Interfaces* **2020**, *12*, 4558–4564.
- (31) Cota, L. G.; de la Mora, P. On the structure of lithium peroxide, Li_2O_2 . *Acta Cryst. B* **2005**, *61*, 133–136.
- (32) Enkovaara, J. et al. Electronic structure calculations with GPAW: a real-space imple-

- mentation of the projector augmented-wave method. *Journal of Physics: Condensed Matter* **2010**, *22*.
- (33) Mekonnen, Y. S.; Garcia-Lastra, J. M.; Hummelshøj, J. S.; Jin, C.; Vegge, T. Role of Li₂O₂@Li₂CO₃ Interfaces on Charge Transport in Nonaqueous Li–Air Batteries. *The Journal of Physical Chemistry C* **2015**, *119*, 18066–18073.
- (34) Mathiesen, N. R.; Yang, S.; García-Lastra, J. M.; Vegge, T.; Siegel, D. J. Charge Transport in Alkali-Metal Superoxides: A Systematic First-Principles Study. *Chem. Mater.* **2019**, *31*, 9156–9167.
- (35) Johnson, L.; Li, C.; Liu, Z.; Chen, Y.; Freunberger, S. A.; Ashok, P. C.; Praveen, B. B.; Dholakia, K.; Tarascon, J.-M.; Bruce, P. G. The role of LiO₂ solubility in O₂ reduction in aprotic solvents and its consequences for Li–O₂ batteries. *Nat. Chem* **2014**, *6*, 1091–1099.
- (36) Tian, F.; Radin, M. D.; Siegel, D. J. Enhanced Charge Transport in Amorphous Li₂O₂. *Chem. Mater.* **2014**, *26*, 2952–2959.
- (37) Li, S.; Liu, J.; Liu, B. First-Principles Study of the Charge Transport Mechanisms in Lithium Superoxide. *Chem. Mater.* **2017**, *29*, 2202–2210.